

CHROMIUM SULFIDE SYNTHESIS AND LITHIATION/DELITHIATION ANALYSIS

By

Jacob Henry Bogenschuetz

Bachelor of Science, University of Wisconsin - Whitewater, 2016

A Thesis

Submitted to the Graduate Faculty

of the

University of North Dakota

in partial fulfillment of the requirements

for the degree of

Master of Science

Grand Forks, North Dakota


December

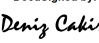
2021

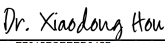
Copyright 2021 Jacob Bogenschuetz

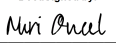
Name: Jacob Bogenschuetz
Degree: Master of Science

This document, submitted in partial fulfillment of the requirements for the degree from the University of North Dakota, has been read by the Faculty Advisory Committee under whom the work has been done and is hereby approved.

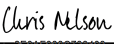
DocuSigned by:

D0E6B634327947F...
Kanishka Marasinghe

DocuSigned by:

E44763F9A06D49B...
Deniz Cakir

DocuSigned by:

E7615FC6EEED945B...
Xiaodong Hou

DocuSigned by:

F42D61CB47C3491...
Oncel Nuri

This document is being submitted by the appointed advisory committee as having met all the requirements of the School of Graduate Studies at the University of North Dakota and is hereby approved.

DocuSigned by:

2E0A7088C733403...
Chris Nelson
Dean of the School of Graduate Studies

12/2/2021
Date

PERMISSION

Title CHROMIUM SULFIDE SYNTHESIS AND LITHIATION/DELITHIATION
 ANALYSIS

Department Physics and Astrophysics

Degree Master of Science

In presenting this thesis in partial fulfillment of the requirements for a graduate degree from the University of North Dakota, I agree that the library of this University shall make it freely available for inspection. I further agree that permission for extensively copying for scholar purposes may be granted by the professor who supervised my thesis work on, in his absence, by the Chairperson of the department of the dean of the School of Graduate Studies. It is understood that any copying or publication or other use of this thesis or part thereof for financial gain shall not be allowed without my written permission. It is also understood that due recognition shall be given to me and to the University of North Dakota in any scholarly use which may be made of any material in my thesis.

Jacob H Bogenschuetz

Date

TABLE OF CONTENTS

LIST OF FIGURES.....	vii
ACKNOWLEDGMENTS.....	x
ABSTRACT.....	xii
CHAPTER	
I. INTRODUCTION AND MOTIVATION.....	1
II. REVIEW ON LITHIUM-ION BATTERIES (LIBs).....	4
III. BARRIERS AND DIFFICULTIES.....	6
IV. ANODE MATERIALS.....	8
V. MATERIAL SYNTHESIS.....	9
5.1. MOTEVATION.....	9
5.2. SYNTHESIS PROCEDURES.....	10
VI. EXPERIMENTAL PROCEDURES.....	12
6.1. INTRODUCTION.....	12
6.2. REACTION VESSEL.....	12
6.3. XPS ANALYSIS.....	12

6.4. XRD ANALYSIS.....	14
6.5. BATTERY FABRICATION.....	15
VII. RESULTS AND DISCUSSION.....	17
7.1. XRD.....	17
7.2. XPS.....	18
VIII. CONCLUSION.....	26
IX. REFERENCES.....	27

LIST OF FIGURES

<i>Figure 1.1: Transition metals highlighted in blue, chalcogenides highlighted in orange.....</i>	<i>2</i>
<i>Figure 1.2: Figure 1.2: Structure of Cr₂S₃. Left is the side view along with <100> direction of a single unit cell. Right is the top view of the same material.....</i>	<i>3</i>
<i>Figure 2.1: Illustration of lithium-Ion battery.....</i>	<i>4</i>
<i>Figure 2.2: Illustration of Electrolyte window and relative reductant/oxidant chemical potential (μ_A/μ_B) positions, respectively.....</i>	<i>5</i>
<i>Figure 5.1: Illustration of sealed quartz tube to be heated in a furnace for the thermal reaction of chromium and sulfur.....</i>	<i>10</i>
<i>Figure 6.1: Basic concept of an electron multiplier.....</i>	<i>14</i>
<i>Figure 6.2: Diagram of XRD diffraction and Bragg's Law.....</i>	<i>15</i>
<i>Figure 6.3: Illustrates the chemical formula of the electrolyte (left) and the binder (right).....</i>	<i>16</i>

Figure 6.4: Illustrates the process of lithiation introducing additional lithium toward the cathode and extraction of lithium in the form of Lithium fluoride (LiF) through delithiation.....16

Figure 7.1: XRD results measured on different samples at various stages of discharging.17

Figure 7.2: Status of electrode samples 9, 10, 11. As seen, electrodes exhibit a uniform lithiation curve (seen in black), and a delithiation curve to a point unique for each electrode (seen in red). Points indicated for the lithiation curve are for representation.....18

Figure 7.3: Illustrates the relative concentration of Li/F/P/C/O. O and C increase in sample 11. Conversely, Li and F decrease.....19

Figure 7.4: Left; Relative concentration percentage Li, F, P. Right; corresponding graphic20

Figure 7.5: Illustrates the multiplex data of Li 1s peak for each sample. Concentration indicates the relative concentration of Li for that sample vs F and P. Possible sources of lithium are the electrolyte and the counter anode.....21

Figure 7.6: Illustrates the multiplex data of fluorine for each sample. Concentration indicates the relative concentration of fluorine compounds for that sample vs lithium and phosphorus. Possible initial sources of fluorine are the electrolyte and the binder.....22

Figure 7.7: Illustrates the multiplex data of phosphorus for each sample. Concentration indicates the relative concentration of phosphorus compounds for that sample vs lithium and fluorine. The only possible source of phosphorus is the electrolyte.....23

Figure 7.8: Illustrates the relative concentrations of the elements Lithium, Fluorine, and Phosphorous and their compositions.....25

ACKNOWLEDGMENTS

I wish to express my sincere appreciation to the members of my Advisory Committee for their guidance and support during my time in the master's program at the University of North Dakota.

To my parents

ABSTRACT

Lithium-Ion Batteries (LIBs) have quickly become a cornerstone of the modern electronics industry, with applications in personal electronic devices, automotive components, and several other areas of interest. With global demand for energy-storing capacity and clean energy solutions only expected to increase in the coming years, developing high-capacity LIB technology has become a priority in battery-related research. A promising method for scaling LIB technology is the use of transition metal chalcogenides (TMCs) as high-capacity anode materials. A number of important physical properties make TMCs favorable for LIB materials such as high thermal conductivity, storage capacity, and rapid charge transfer. This experiment began with the synthesis of the TMC chromium sulfide (Cr_2S_3) via thermal synthesis. After this process, the materials were analyzed via X-ray Photoelectron Spectroscopy (XPS) and X-ray Powder Diffraction (XRD) methods to determine the chemical composition of each sample. We built and tested half-cell coin batteries to evaluate the performance of this material. To study the details of lithiation and delithiation, XPS and XRD measurements were conducted on the electrode material at various stages of the process. The results of these experiments not only confirmed the formation of the Solid Electrolyte Interface (SEI) layer but also provided details of its chemical composition.

CHAPTER I

INTRODUCTION AND MOTIVATION

As modern technology advances, the demand for high-performance batteries increases proportionally. This, in turn, drives scientific research into various battery properties, including cost, safety, rechargeability, cycling life, voltage, capacity, and rate capability. The perpetual rise in global energy demands has made the use of fossil fuels increasingly problematic. Many potential solutions have been proposed for this problem; chief among these is the use of energy harvested from renewable resources, such as solar and wind, which can then be stored via stationary rechargeable batteries.

The emergence of the lithium-ion rechargeable battery (LIB) has allowed unprecedented advances in portable electronic devices (e.g. laptops and cell phones) and continues to revolutionize communication. The pressing issue to be solved with regards to LIBs and similar technology is the ability to ensure a low-cost, sustainable energy storage solution. Furthermore, it is becoming increasingly apparent that LIB technology can help phase out the internal combustion engine through the implementation of LIBs in electric vehicles, and in-home power storage. Examples of companies on the frontier of this technology include Tesla and solar city.

To meet energy demands and improve performance, battery electrode materials are of great interest. One promising class of anode materials for the advance in LIBs is transition metal chalcogenides (TMCs). TMCs as anode materials have unique and

promising properties (e.g., thermal conductivity, abundance, and fast charge transfer kinetics).^[24] Currently, the most used anode material in LIBs is graphite. However, graphite has certain limitations for which TMCs show promise to overcome. This advantage provides abundant motivation for research into alternative anode materials that allow higher energy density in LIBs.

Periodic Table of the Elements

Periodic Table of the Elements																																																			
1 IA	2 IIA 2A												13 IIIA 3A	14 IVA 4A	15 VA 5A	16 VIA 6A	17 VIIA 7A	18 VIIIA 8A																																	
1 H Hydrogen 1.008													5 B Boron 10.811	6 C Carbon 12.011	7 N Nitrogen 14.007	8 O Oxygen 15.999	9 F Fluorine 18.998	10 Ne Neon 20.180																																	
3 Li Lithium 6.941	4 Be Beryllium 9.012											11 Na Sodium 22.990	12 Mg Magnesium 24.305											13 Al Aluminum 26.982	14 Si Silicon 28.086	15 P Phosphorus 30.974	16 S Sulfur 32.06	17 Cl Chlorine 35.453	18 Ar Argon 39.948																						
19 K Potassium 39.098	20 Ca Calcium 40.078	21 Sc Scandium 44.956	22 Ti Titanium 47.88	23 V Vanadium 50.942	24 Cr Chromium 51.996	25 Mn Manganese 54.938	26 Fe Iron 55.845	27 Co Cobalt 58.933	28 Ni Nickel 58.693	29 Cu Copper 63.546	30 Zn Zinc 65.39	31 Ga Gallium 69.723	32 Ge Germanium 72.61	33 As Arsenic 74.922	34 Se Selenium 78.972	35 Br Bromine 79.904	36 Kr Krypton 83.80																																		
37 Rb Rubidium 85.468	38 Sr Strontium 87.62	39 Y Yttrium 88.906	40 Zr Zirconium 91.224	41 Nb Niobium 92.906	42 Mo Molybdenum 95.94	43 Tc Technetium 98.906	44 Ru Ruthenium 101.07	45 Rh Rhodium 102.905	46 Pd Palladium 106.42	47 Ag Silver 107.868	48 Cd Cadmium 112.411	49 In Indium 114.818	50 Sn Tin 118.71	51 Sb Antimony 121.760	52 Te Tellurium 127.6	53 I Iodine 126.905	54 Xe Xenon 131.29																																		
55 Cs Cesium 132.905	56 Ba Barium 137.327	57-71 Lanthanide Series	72 Hf Hafnium 178.49	73 Ta Tantalum 180.948	74 W Tungsten 183.85	75 Re Rhenium 186.207	76 Os Osmium 190.23	77 Ir Iridium 192.22	78 Pt Platinum 195.08	79 Au Gold 196.967	80 Hg Mercury 200.59	81 Tl Thallium 204.383	82 Pb Lead 207.2	83 Bi Bismuth 208.980	84 Po Polonium (209)	85 At Astatine (210)	86 Rn Radon 222.018																																		
87 Fr Francium 223.021	88 Ra Radium 226.025	89-103 Actinide Series	104 Rf Rutherfordium (261)	105 Db Dubnium (262)	106 Sg Seaborgium (266)	107 Bh Bohrium (264)	108 Hs Hassium (265)	109 Mt Meitnerium (268)	110 Ds Darmstadtium (271)	111 Rg Roentgenium (272)	112 Cn Copernicium (285)	113 Nh Nihonium (284)	114 Fl Flerovium (289)	115 Uup Ununpentium (288)	116 Lv Livermorium (293)	117 Uus Ununseptium (289)	118 Uuo Ununoctium (294)																																		
<table border="1"> <thead> <tr> <th colspan="2">Lanthanide Series</th> </tr> </thead> <tbody> <tr> <td>57 La Lanthanum 138.905</td> <td>58 Ce Cerium 140.115</td> <td>59 Pr Praseodymium 140.908</td> <td>60 Nd Neodymium 144.24</td> <td>61 Pm Promethium 144.913</td> <td>62 Sm Samarium 150.36</td> <td>63 Eu Europium 151.965</td> <td>64 Gd Gadolinium 157.25</td> <td>65 Tb Terbium 158.925</td> <td>66 Dy Dysprosium 162.50</td> <td>67 Ho Holmium 164.930</td> <td>68 Er Erbium 167.26</td> <td>69 Tm Thulium 168.934</td> <td>70 Yb Ytterbium 173.04</td> <td>71 Lu Lutetium 174.967</td> </tr> </tbody> </table> <table border="1"> <thead> <tr> <th colspan="2">Actinide Series</th> </tr> </thead> <tbody> <tr> <td>89 Ac Actinium 227.028</td> <td>90 Th Thorium 232.038</td> <td>91 Pa Protactinium 231.036</td> <td>92 U Uranium 238.029</td> <td>93 Np Neptunium 237.048</td> <td>94 Pu Plutonium 244.064</td> <td>95 Am Americium 243.061</td> <td>96 Cm Curium 247.070</td> <td>97 Bk Berkelium 247.070</td> <td>98 Cf Californium 251.080</td> <td>99 Es Einsteinium 252</td> <td>100 Fm Fermium 257.095</td> <td>101 Md Mendelevium 258.1</td> <td>102 No Nobelium 259.101</td> <td>103 Lr Lawrencium 262</td> </tr> </tbody> </table>																		Lanthanide Series		57 La Lanthanum 138.905	58 Ce Cerium 140.115	59 Pr Praseodymium 140.908	60 Nd Neodymium 144.24	61 Pm Promethium 144.913	62 Sm Samarium 150.36	63 Eu Europium 151.965	64 Gd Gadolinium 157.25	65 Tb Terbium 158.925	66 Dy Dysprosium 162.50	67 Ho Holmium 164.930	68 Er Erbium 167.26	69 Tm Thulium 168.934	70 Yb Ytterbium 173.04	71 Lu Lutetium 174.967	Actinide Series		89 Ac Actinium 227.028	90 Th Thorium 232.038	91 Pa Protactinium 231.036	92 U Uranium 238.029	93 Np Neptunium 237.048	94 Pu Plutonium 244.064	95 Am Americium 243.061	96 Cm Curium 247.070	97 Bk Berkelium 247.070	98 Cf Californium 251.080	99 Es Einsteinium 252	100 Fm Fermium 257.095	101 Md Mendelevium 258.1	102 No Nobelium 259.101	103 Lr Lawrencium 262
Lanthanide Series																																																			
57 La Lanthanum 138.905	58 Ce Cerium 140.115	59 Pr Praseodymium 140.908	60 Nd Neodymium 144.24	61 Pm Promethium 144.913	62 Sm Samarium 150.36	63 Eu Europium 151.965	64 Gd Gadolinium 157.25	65 Tb Terbium 158.925	66 Dy Dysprosium 162.50	67 Ho Holmium 164.930	68 Er Erbium 167.26	69 Tm Thulium 168.934	70 Yb Ytterbium 173.04	71 Lu Lutetium 174.967																																					
Actinide Series																																																			
89 Ac Actinium 227.028	90 Th Thorium 232.038	91 Pa Protactinium 231.036	92 U Uranium 238.029	93 Np Neptunium 237.048	94 Pu Plutonium 244.064	95 Am Americium 243.061	96 Cm Curium 247.070	97 Bk Berkelium 247.070	98 Cf Californium 251.080	99 Es Einsteinium 252	100 Fm Fermium 257.095	101 Md Mendelevium 258.1	102 No Nobelium 259.101	103 Lr Lawrencium 262																																					

Figure 1.1: Transition metals highlighted in blue, chalcogenides highlighted in orange.

This research focused on Cr_2S_3 and the physical and chemical changes through the lithiation and delithiation process. The material was then synthesized thermally in vacuum-sealed quartz tubes according to the literature.^[18] After synthesis, the material was characterized via X-ray Diffraction (XRD), X-ray Photoelectron Spectroscopy (XPS), and Atomic Force Microscopy (AFM) to ensure purity and uniformity.

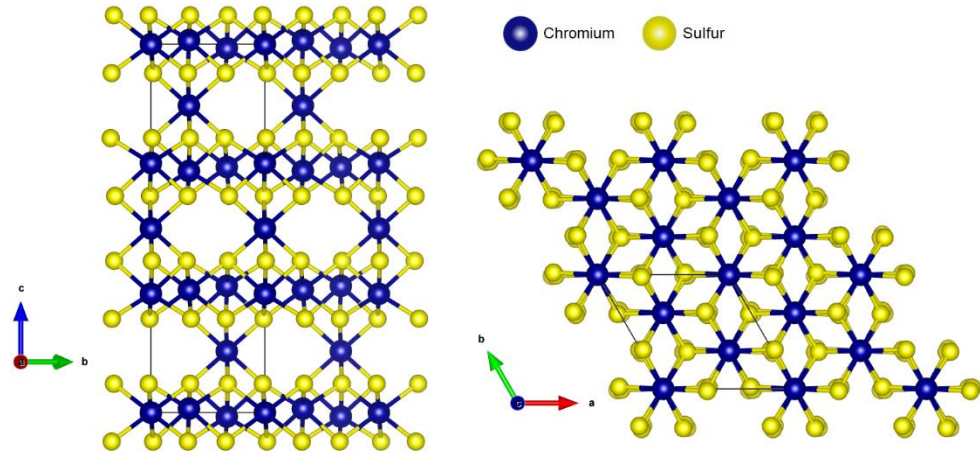


Figure 1.2: Structure of Cr_2S_3 . Left is the side view along with $\langle 100 \rangle$ direction of a single unit cell. Right is the top view of the same material.

CHAPTER II

REVIEW ON LITHIUM-ION BATTERIES (LIBS)

A modern lithium-ion battery is a rechargeable battery composed of a lithium-based electrolyte (e.g. LiPF_6), lithium compound cathode (e.g. LiFePO_4), and a carbon anode.^[2] Chemical potential drives a chemical reaction, which causes lithium ions to act as a charge carrier within the battery cell. Simultaneously, electrons do work outside the cell due to the potential difference that is present.^[2] The most common anode material is carbon and its derivatives.^[2]

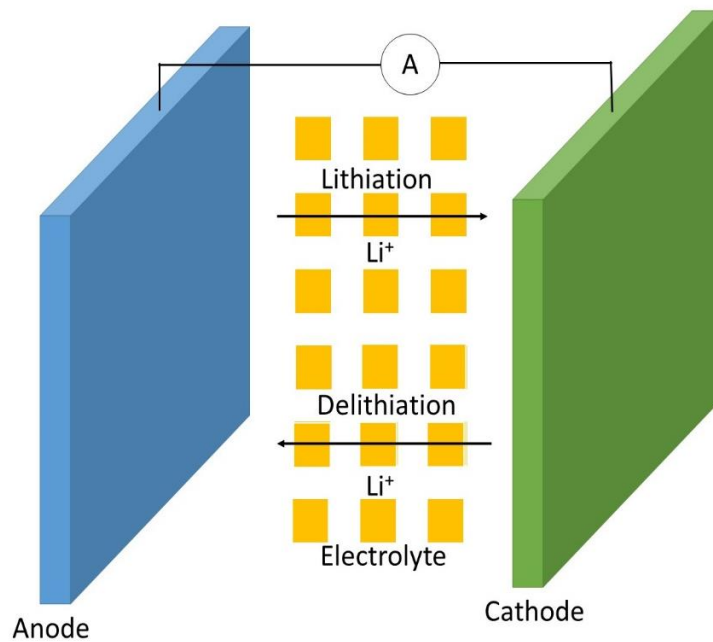


Figure 2.1: Illustration of lithium-Ion battery

The voltage of the cell is the difference in chemical potential between the two electrodes. For a battery to operate properly the chemical potential of each electrode

must remain within the electrolyte window. If the chemical potential of either electrode is not within the electrolyte window, reactions anterior to the battery's intended mechanism will occur.^[6] If this happens, the electrolyte may be reduced at the anode or oxidized at the cathode. These reactions can adversely affect battery performance; furthermore, this may lead to catastrophic battery failure.

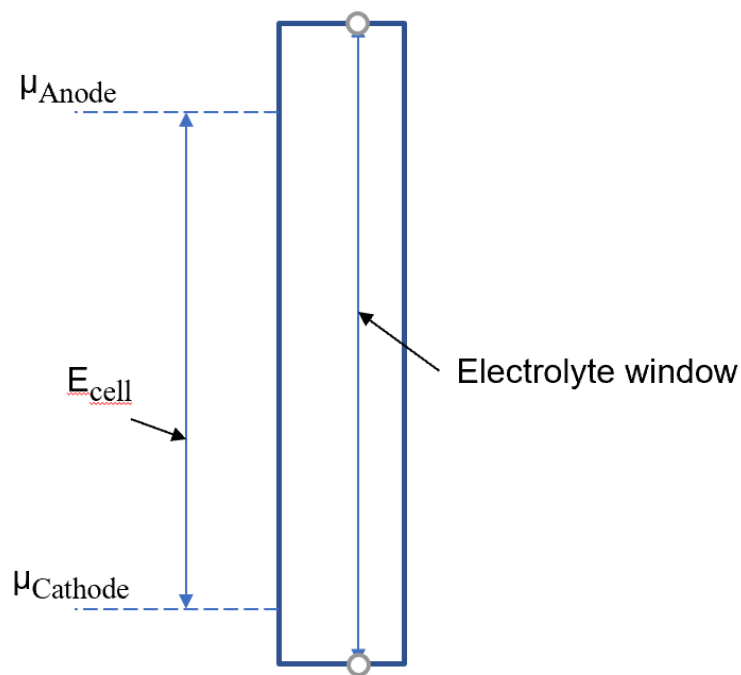


Figure 2.2: Illustration of Electrolyte window and relative reductant/oxidant chemical potential (μ_A/μ_B) positions, respectively.

CHAPTER III

BARRIERS AND DIFFICULTIES

Some of the largest barriers in the way of modern LIB technology are the high cost of materials, the limited cycle lifespan, and issues regarding safety.^[2] Irreversible chemical changes during charge/discharge cycles can lead to capacity degradation and dangerous conditions.^[24]

One mode of irreversible chemical change is the shuttle effect. The shuttle effect occurs as a result of a series of steps, the first of which is the formation of dendrites. These dendrites consist of long chains of material branching out from the electrode. These dendrites themselves can be very dangerous and can lead to catastrophic failure. The second step in the process of the shuttle effect is the detaching of sections of this dendrite chain from the electrode host. Next, these chain sections diffuse into the electrolyte; this is followed by the migration of these chain sections toward the opposite electrode. Lastly, these chains react with the opposite electrode and form a new material.^[14] Another possible effect of dendrites is that they can create electrical short circuits within the battery that can lead to overheating and explosion.

Another mode of irreversible changes in the battery cell is volume expansion and contraction. Volume expansion in experimental batteries has been observed to be as great as 80% during the charge/discharge cycle. These volume changes can result in the

separation of materials with the battery. This leads to a strongly reduced cycle life, rate performance, capacity, and safety of the cell.^[24]

A common risk to the battery cell life and health is overcharging. This can also be dangerous and can even lead to catastrophic failure. This can irreversibly damage the battery by way of gas production and build-up, rapid temperature increase, and chemical changes within the cell. The chemical reactions within the cell can lead to catastrophic failure and explosion.^[2]

One method to protect the battery from overcharging is known as a redox shuttle; this is an additive to the electrolyte. This additive can be oxidized or reduced reversibly within a specific potential. This protects from overcharging by allowing a reversible reaction to occur with the redox shuttle rather than other potential irreversible reactions.^[2] In industry, over-charging is also mitigated through a battery management system (BMS).^[17]

To address the problems mentioned above, there are several key drivers for the research of new battery materials. Current LIBs need improvement to keep up with or even meet current energy storage demands. For applications such as grid storage, current LIB technology proves to be insufficient due to the cost of materials and performance limitations.^[12] With the rising popularity of LIBs and LIB technology, the sourcing of lithium is becoming a topic of concern.^[22] To help with that, recently the research has been focused on Na-ion batteries (SIB).

CHAPTER IV

ANODE MATERIALS

Anode materials have been of great interest in the advancement of lithium battery technology.^[24,25,21,11] Specific capacity is perhaps the most interesting driver of research into new anode materials. The specific capacity of the current commercial graphite (common carbon anode) is 372 mAh g⁻¹.^[21] Carbon also has poor low-temperature performance. These issues strongly limit the capacity of current LIBs. For comparison, the theoretical capacity for some investigated TMCs has been near or more than 1000 mAh g⁻¹.^[24,25] The potential for these materials to revolutionize modern battery technology is astounding. Many materials have been explored as possible anode materials, including carbon materials, silicon, metals, and Transition Metal Chalcogenides (TMCs).^[12]

There are three primary storage mechanisms for anode materials. Intercalation anodes present a rigid molecular structure that allows lithiation and delithiation while maintaining that structure; graphite is one such intercalation anode.^[12] A conversion anode chemically reacts with the Li-ion carrier to form a new compound with a new structure.^[22] TMC anodes are an example of conversion anodes.^[12] The third type is called alloy anodes such as Si, Ge and Sn. Alloying anodes undergo reactions that involve major structural changes.^[24]

CHAPTER V

MATERIAL SYNTHESIS

5.1. MOTIVATION

Transition metal chalcogenides especially sulfides and selenides have attracted a lot of attention for LIB and SIB applications because of their unique physical and chemical properties such as high electrical conductivity, thermal stability, etc. In addition to that, transition metal chalcogenides offer higher theoretical specific capacities for LIB/SIBs compared to commonly used intercalation anodes. Another important point to make is that transition metal chalcogenides are electrochemically more reversible than their metal oxide counterparts due to the faster charge transfer kinetics. For example, metal sulfides such as MoS_2 ²⁰, CoS_2 ⁴, SnS ¹⁰, Sb_2S_3 ¹⁶, and FeS_2 ²³ have shown great potential as anode materials for LIBs/SIBs because of their higher volume capacity and better rate performance resulting from higher density and electrical conductivity. However, there are still unknowns regarding the effect of lithiation and delithiation process on the electrodes.

Various transition metal chalcogenides have been investigated for anode material in Li-ion batteries. The research on CrS , Li_zCrS_2 compounds showed that the lithiation and delithiation processes of these materials are not reversible.^[8,9] However, nobody studied Cr_2S_3 . We were motivated by the lack of research on the performance of Cr_2S_3 as an electrode. Ultimately, we want to correlate how the performance of a material is affected by the composition and structure of the material.

5.2. SYNTHESIS PROCEDURES

Cr_2S_3 synthesis methodology was modified through trial and error from previously reported research.^[18] To maintain the desired reaction, a pressure below 10^{-3} Torr must be maintained throughout the five-day reaction period. Any amount of leakage - even a minute flow of inert argon gas - will allow gaseous sulfur to escape, disrupting the stoichiometric mixture. Therefore, a stoichiometric mixture of chromium and sulfur was sealed in an evacuated silica tube ($<10^{-3}$ Torr) at 500°C for 24 hours. The furnace temperature was then adjusted to 1000°C for 96 hours, then allowed to cool naturally in the furnace to room temperature. After cooling, the material was removed from the sealed tube and examined with XPS.

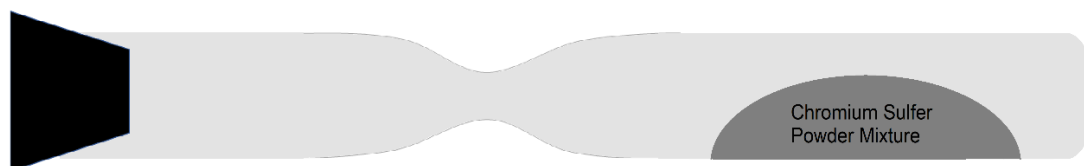


Figure 5.1: Illustration of sealed quartz tube to be heated in a furnace for the thermal reaction of chromium and sulfur

During the reaction, the vaporization of sulfur causes enough pressure to accumulate that the tubes can explode under certain circumstances. The greatest contributor to explosions is tube sizing; a tube size that is too small relative to the material

quantity may be very hazardous. Other possible causes of explosion include weakening of the glass structure through rapid heating and cooling, as well as defects formed on quartz during the sealing process.

CHAPTER VI

EXPERIMENTAL PROCEDURES

6.1. INTRODUCTION

Following is a summary of the experimental procedures used in this research. This includes an overview of the reaction vessels used, a discussion of heat treatments and post-reaction processes, and a description of the various analysis techniques employed in research (i.e. X-ray diffractometer, X-ray photoelectron spectroscopy). Furthermore, an exploration of battery testing used in this research through the UND Chemical Engineering Department is elaborated on.

6.2. REACTION VESSEL

For this experiment, a quartz tube was used. Quartz was favored for a tube material because it can tolerate the high temperatures (i.e. up to 1000 °C) required for the material synthesis to occur; quartz features a melting point of roughly 1600 °C.

After the samples have been synthesized, they are collected for X-ray photoelectron spectroscopy (XPS) analysis, and later, X-ray diffraction (XRD) analysis.

6.3. XPS ANALYSIS

XPS was developed by Swedish Dr. Kai Siegbahn and his collaborators in the 1960s; this revolutionary method later won Dr. Siegbahn a Nobel Prize in Physics. XPS is used to determine the chemical composition of the samples analyzed. XPS is performed by exposing the surface of a sample with X-rays, emitted from an X-ray source, and capturing the electrons emitted by the surface via the photoelectric effect. As an electron source,

a Ti filament is used. Then, electrons are accelerated towards and Al target via a potential difference. The aluminum target, when bombarded by high-energy electrons, produces X-rays that are directed towards the sample.

The X-ray bombardment causes the sample to emit electrons. This is known as the photoelectric effect, and it occurs when electromagnetic energy excites electrons past their work function and binding energies, causing them to be emitted from the sample. These electrons are then captured by the detector. A hemispherical chamber uses a controlled electric field to select electrons of a certain speed to be counted. The electron speed corresponds to the eV range they originate from (E.g. Oxygen 1s orbital electrons have binding energy ~531 eV; AlK α X-rays have photon energy 1486.6eV; detector read kinetic energy of Oxygen 1s electron is ~955.6eV less the spectrometer work function).^[13] The number of electrons roughly corresponds to the number of atoms on the surface of the material.

$$KE \approx h\nu - BE - \phi$$

h ν (photon energy)

KE(measured electron kinetic energy)

BE(binding energy of orbital electron originates from)

ϕ (spectrometer work function)

An electron multiplier amplifies the signal and sends it to the XPS electronics.^[19]

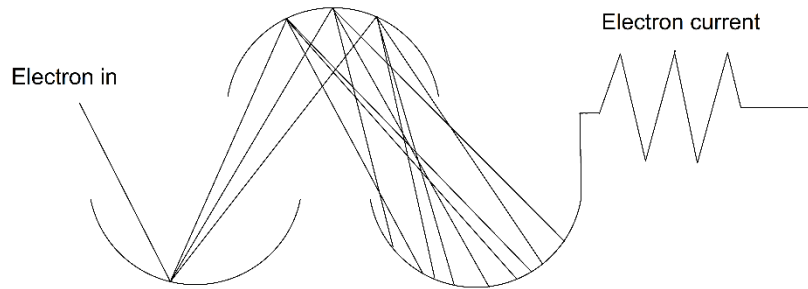


Figure 6.1 Basic concept of an electron multiplier

6.4. XRD ANALYSIS

X-ray Diffraction (XRD) analysis was used to verify the purity of the active anode material (Cr_2S_3). XPS is primarily used to determine the chemical composition of a sample, whereas XRD analysis reveals the crystal structure.

In XRD, elastically scattered X-rays are detected. Within a crystal structure, there are very specific angles in which the scattered X-rays will constructively interfere. This is referred to as diffraction. From the scattering angles measured by XRD, the crystal structure and lattice spacing can be extracted.

XRD uses Bragg's Law which describes the relationship between X-ray behavior and the material's crystalline structure. Bragg's Law is stated as

$$2d\sin\theta = m\lambda$$

where d , λ , and θ are interplanar spacing, the wavelength of the X-ray and angle of incidence, respectively, and m is a dimensionless integer.

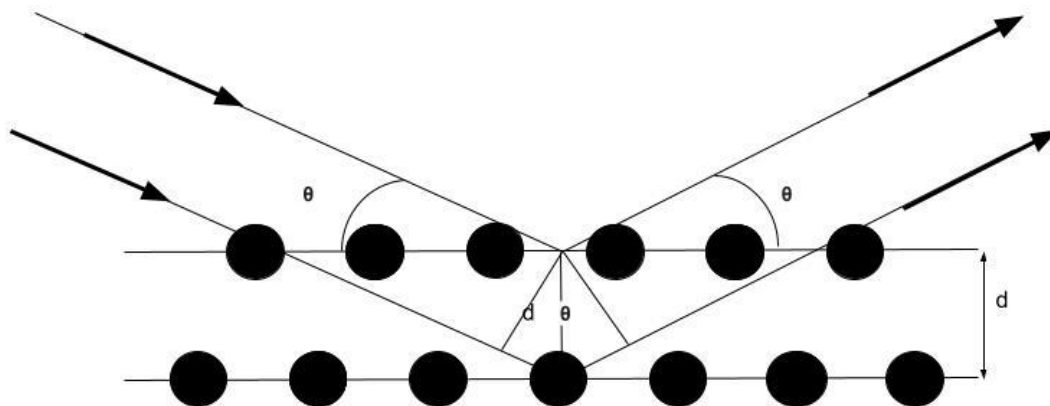


Figure 6.2: Diagram of XRD diffraction and Bragg's Law

6.5. BATTERY FABRICATION and TESTING

The batteries were fabricated by a fellow graduate student Shuai Xu in the Institute for Energy Studies at UND. A coin cell setup was created consisting of a CR2032-type coin half-cell assembled in a glove box, with a high-purity argon environment used for its inert nature. In this configuration, the Li counter electrode acts as an anode, and Cr_2S_3 electrode functions as a cathode. For XRD and XPS experiments, two sample sets (six samples in total) were prepared and tested as battery anodes. These samples were made using 60% active material, 20% active carbon, and 20% PVDF binder. The electrolyte is composed of Ethylene Carbonate (EC), Ethyl Methyl Carbonate (EMC), and LiPF_6 . The chemical structure of the electrolyte and the binder are given in Figure 6.3. Once assembled, half-cell LIBs are charged. Testing of the batteries involved discharging (i.e. lithiation) followed by charging (delithiation). (See Figure 7.7)

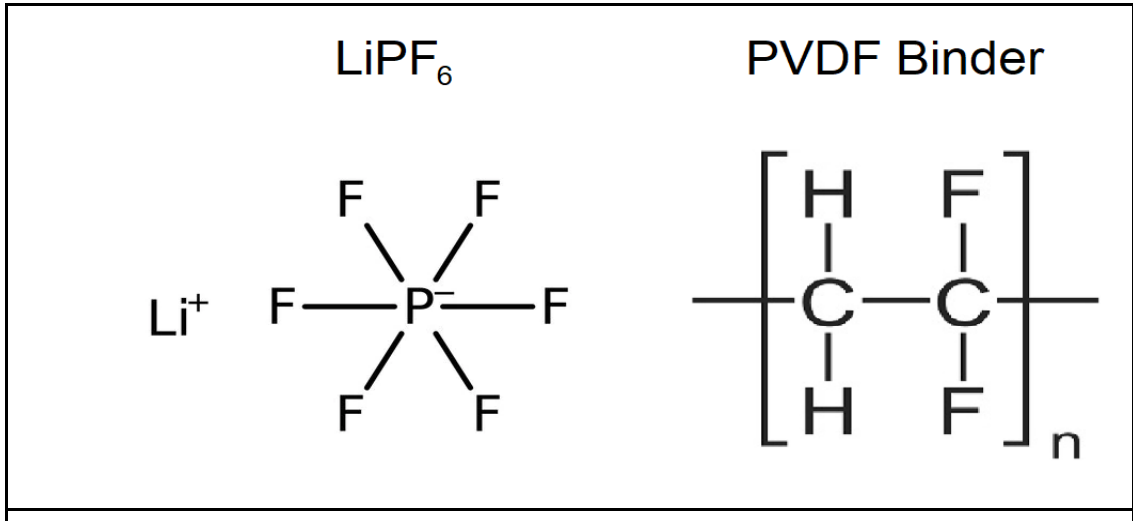


Figure 6.3: Illustrates the chemical formula of the electrolyte (left) and the binder (right)

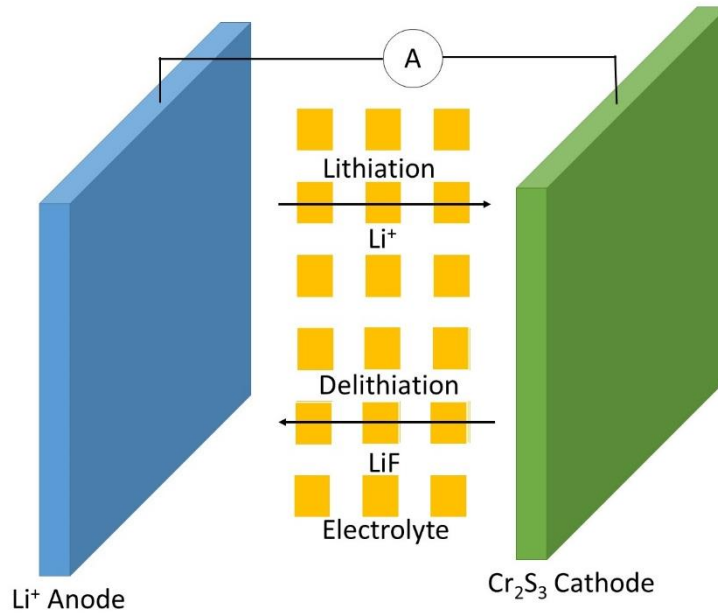


Figure 6.4: Illustrates the process of lithiation introducing additional lithium toward the cathode and extraction of lithium in the form of Lithium fluoride (LiF) through delithiation.

CHAPTER VII

RESULTS & DISCUSSION

7.1 XRD

XRD experiments were performed on three samples at various stages during the discharging. The data shows that through the first discharge cycle, the Cr_2S_3 gradually vanishes as Li_2S forms. The presence of this reaction demonstrates that Cr_2S_3 acts as a conversion electrode.

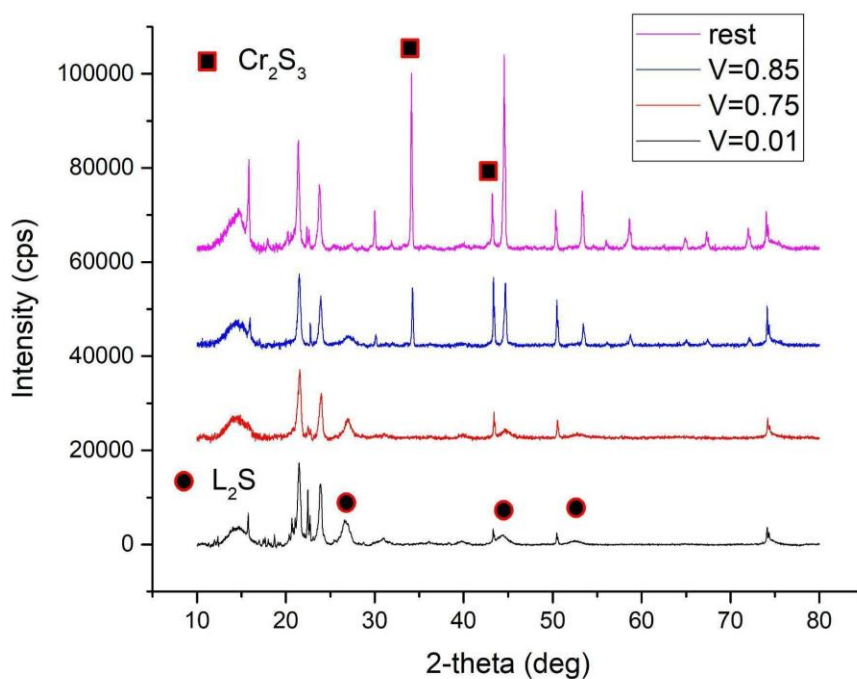


Figure 7.1: XRD results measured on different samples at various stages of discharging.

7.2 XPS

Figure 7.2 shows the Voltage vs Capacity graph. The black-filled circles indicate the state of charging (SOC) of the samples 9, 10, and 11 in the delithiation process.

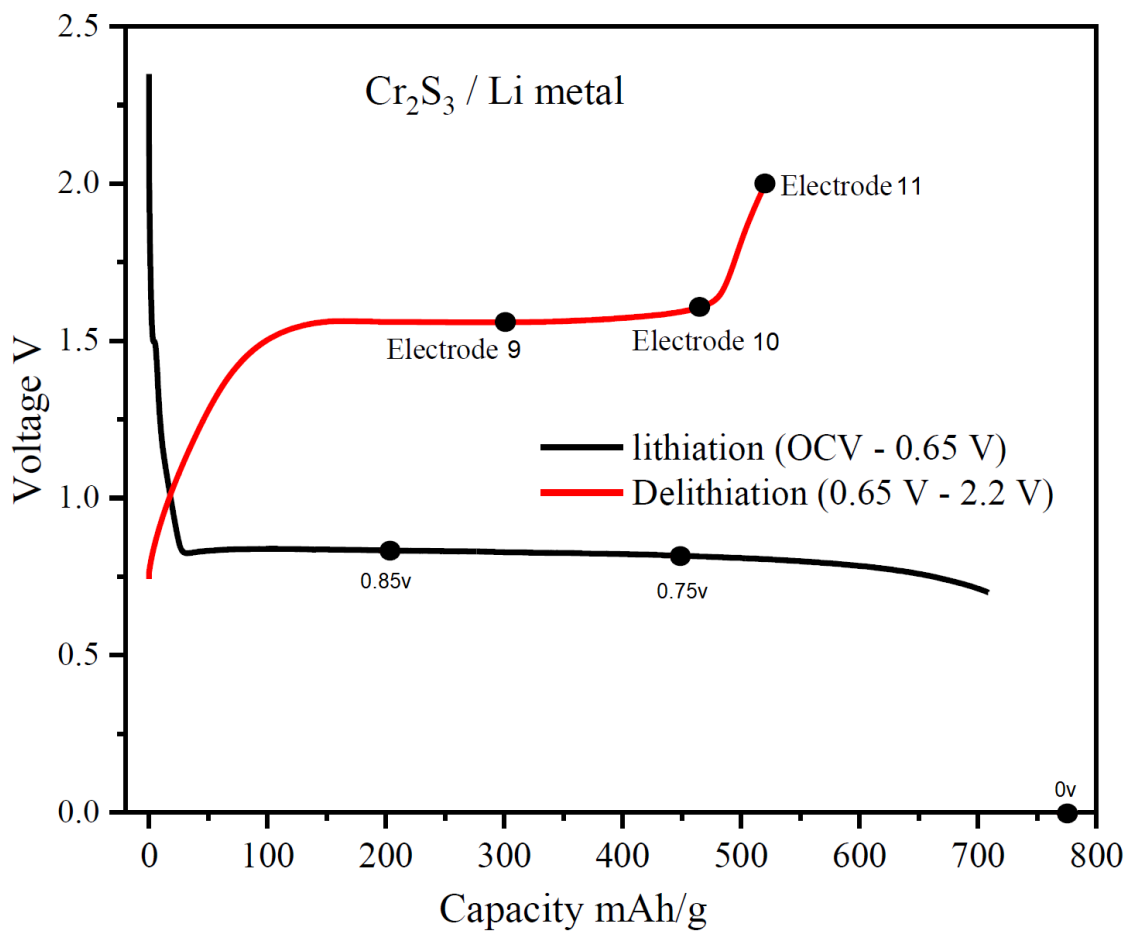


Figure 7.2: Status of electrode samples 9, 10, 11. As seen, electrodes exhibit a uniform lithiation curve (seen in black), and a delithiation curve to a point unique for each electrode (seen in red). Points indicated for the lithiation curve are for representation.

	9	10	11
Li	33.6%	34.6%	22.6%
F	25.9%	35.5%	14.2%
P	5.1%	4.8%	4.1%
C	17%	13%	26.6%
O	18.7%	12%	32.5%

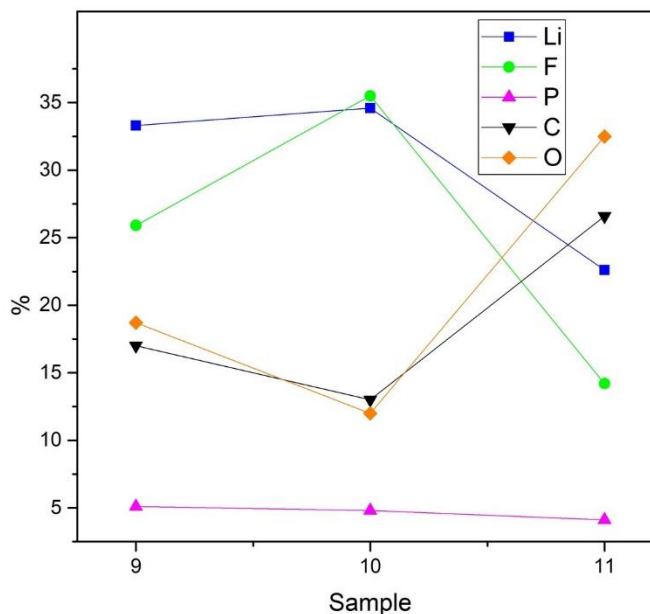


Figure 7.3: Illustrates the relative concentration of Li/F/P/C/O. O and C increase in sample 11. Conversely, Li and F decrease.

Figure 7.3 shows concentrations of Li, F, P, C, and O on samples 9, 10, and 11. The Cr and S concentrations were within the error range in XPS and therefore they were not included in the analysis. The absence of strong Cr and S presence indicates that a relatively thick Solid Electrolyte Interface (SEI) layer must have formed on the electrode preventing access to both Cr and S.^[3] Carbon and Oxygen have many potential sources including exposure to air during the sample transport and loading and therefore their relative intensity can be misleading. However, analysis of Li, F, and P can provide valuable information to explain what may be happening during the delithiation process. The sources of Li, F, and P elements are known. Li has two sources: the electrolyte and the Li counter electrode. F also has two sources: the electrolyte and binder Polyvinylidene

fluoride (PVDF). However, P has one source: the electrolyte. Figure 7.2 shows that during the first delithiation cycle the concentrations of Li, F, and P on the electrode decrease.

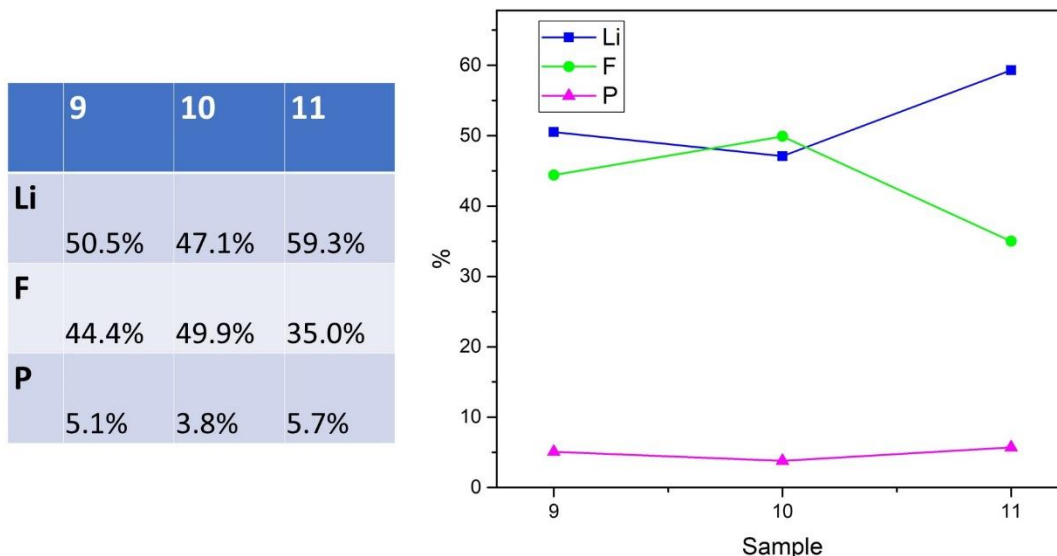


Figure 7.4: Left; Relative concentration percentage Li, F, P. Right; corresponding graphic

To investigate the process further, we focused on relative concentrations of Li, F, and P change during the first delithiation cycle, C and O were not included in this analysis. We performed higher resolution scans on Li 1s, F 1s, and P 2p peaks to investigate if the binding energy and peak composition change during delithiation.

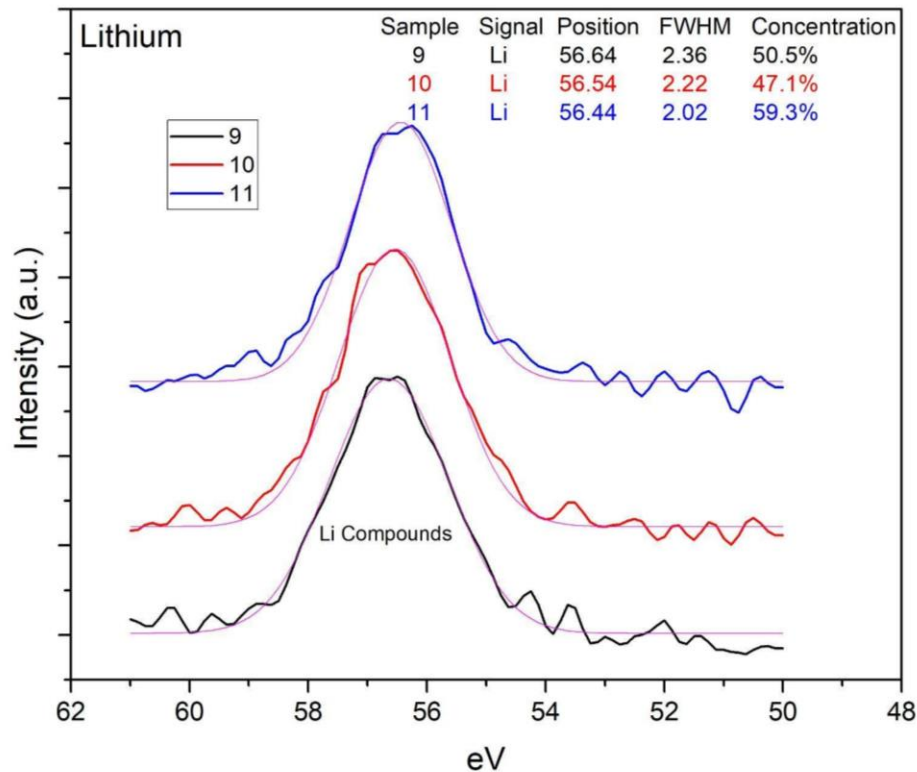


Figure 7.5: Illustrates the multiplex data of Li 1s peak for each sample. Concentration indicates the relative concentration of Li for that sample vs F and P. Possible sources of lithium are the electrolyte and the counter anode.

Li 1s Peak:

For Li, we want to emphasize two important points. The first one is that Li concentration relative to F and P increases. (See Figure 7.4) The second one is that Li 1s peak shows a small but persistent shift to the lower binding energies as the delithiation process continues. (see Figure 7.5) We attribute this shift to the lower binding energy to the formation of Li compounds other than LiF such as Li-carbides and Li-oxides. An increase in Li concentration relative to F concentration indicates that during the

delithiation process, LiF moves from cathode to anode and lowers the concentration of F.

Yet, there remained excess Li that was bound to C and O to form carbides and oxides.

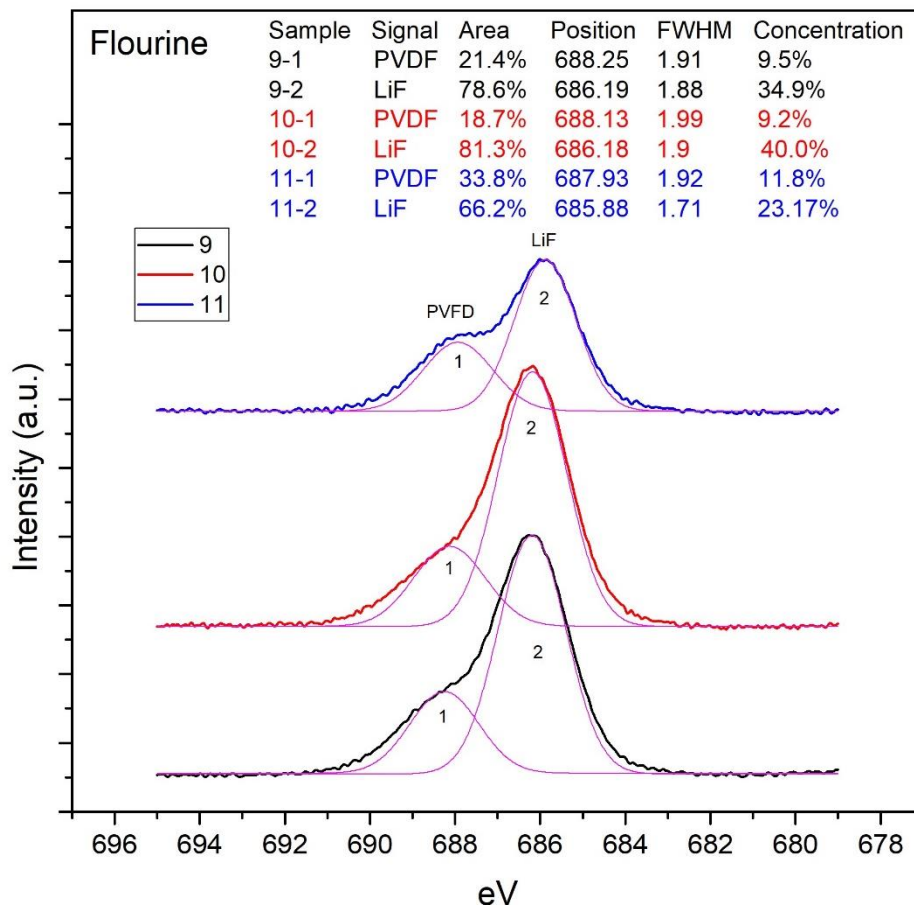


Figure 7.6: Illustrates the multiplex data of fluorine for each sample. Concentration indicates the relative concentration of fluorine compounds for that sample vs lithium and phosphorus. Possible initial sources of fluorine are the electrolyte and the binder.

F 1s Peak:

Figure 7.6 shows F 1s peak for samples 9, 10 and 11. The F peak is composed of two peaks. By using the NIST database and the literature, we attributed the higher binding

energy peak (peak 1) to PVDF and the lower binding energy (Peak 2) to LiF. Figure 7.4 shows that the relative concentration of F with respect to Li decreases sharply from 44.4% in sample 9 to 35.0% in sample 11. However, Figure 7.6 shows that the relative concentrations of PVDF and LiF change independently as the delithiation process continues. When combined, both changes translate to a slight increase of PVDF concentration from 9.5% to 11.8% while LiF concentration decreases sharply from 34.9% to 23.2%. This analysis further suggests the formation of a Solid Electrolyte interface (SEI) layer.

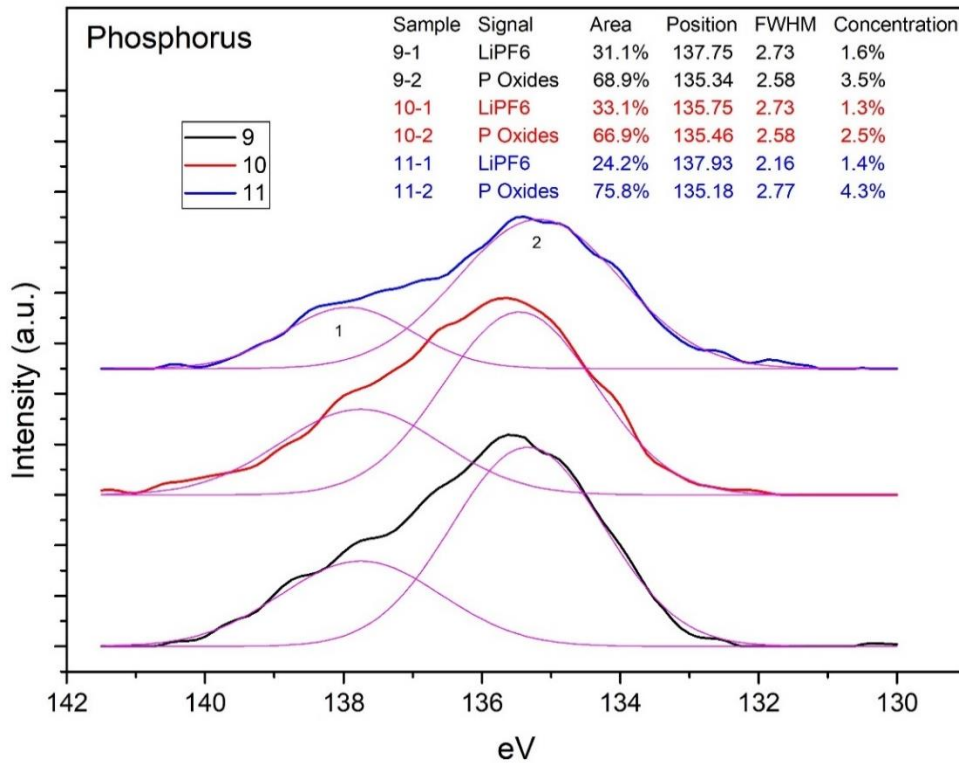


Figure 7.7: Illustrates the multiplex data of phosphorus for each sample. Concentration indicates the relative concentration of phosphorus compounds for that sample vs lithium and fluorine. The only possible source of phosphorus is the electrolyte.

P 2p peak:

To understand what happens to the electrolyte during the delithiation process, we measured higher resolution P 2p peaks for samples 9, 10, and 11. (Figure 7.8) The P 2p peak is composed of two peaks. After comparing our data with the literature, we attributed the primary peak, peak 2, to phosphorus oxides.^[13] and the peak 1 to LiPF_6 , the electrolyte. (See Figure 7.3) The presence of peak 2 indicates that during the process the electrolyte breaks down and P gets oxidized. In sample 9, the total P concentration is 5.1%, and 1.6% of that is in the electrolyte. This means about 1.6% of Li and 9.6% of F shown in Figure 7.4 originates from the electrolyte. This suggests that a majority of the F must come from the LiF. This also indicates the possibility of some of the binder breaking down. On the other hand, the Li supplied by the electrolyte (1.6%) cannot account for all the Li concentrations given in Figure 7.4. Therefore, most of the Li must come from the Li counter electrode and the breakdown of the electrolyte.

In sample 11, P concentration is a bit higher, 5.7%. This means that 5.7% of Li and 34.2% of F must be present. We have significantly more than 5.7% Li, indicating that the majority of Li that came from the anode remained at the cathode. However, we measured only 23% F in the form of LiF meaning that a significant amount of F left the cathode. In light of these results, we think that a Solid Electrolyte Interface (SEI) forms. Excess Li left behind is likely bound to Li_2CO_3 , Li_2O and LiF which are common components known to make up the SEI layer. Further investigation is needed to extract more information on the

chemical composition and structure of these Li-carbide and Li-oxide compounds as well as the underlying mechanism of delithiation in the anode beneath the SEI layer. The samples were exposed to air during the transport between the labs which can lead to the formation of Li-carbides and oxides. To rule out the possibility of contamination, the samples need to be transported under controlled conditions.

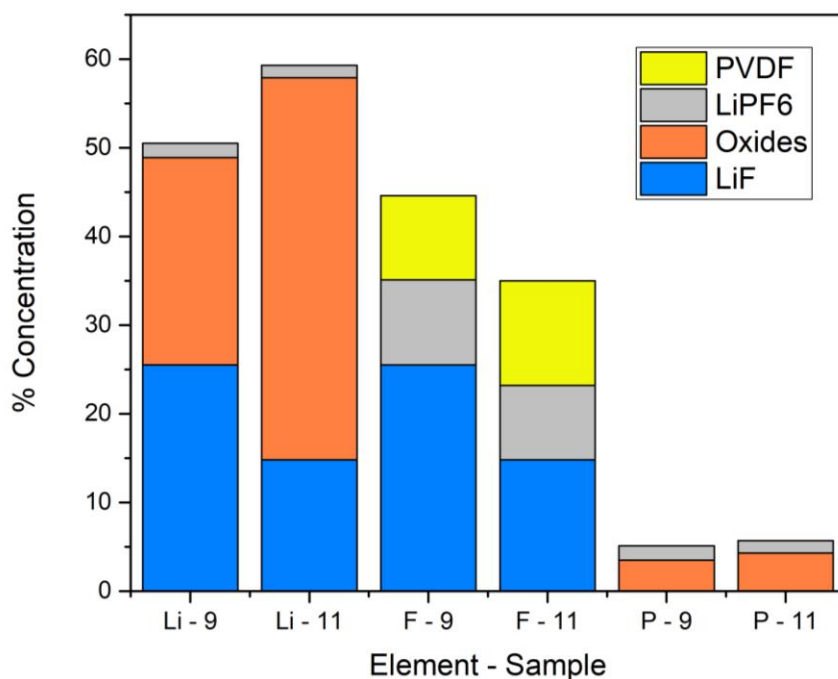


Figure 7.8: Illustrates the relative concentrations of the elements Lithium, Fluorine, and Phosphorous and their compositions.

This leaves high potential for future research. Further examination of the SEI layer under more cycling is necessary to understand, completely, the SEI layer formation for this material. Argon gas sputtering to remove the top SEI layer to investigate the underlying electrode is also necessary to examine the delithiation process within the electrode material.

CHAPTER VIII

CONCLUSION

Lithium-ion batteries (LIBs) are of great importance in the modern electronics industry. An area of particular interest in improving LIB performance is transition metal chalcogenides (TMCs). TMCs show promise as a class of anodic materials in LIBs due to a wide range of favorable physical properties, including thermal conductivity and rapid charge transfer. Here, we focused on the synthesis and analysis of chromium sulfide (Cr_2S_3) as an electrode for LIBs.

Cr_2S_3 is synthesized from a stoichiometric mixture of chromium and sulfur powders. This mixture is kept in a reaction vessel in a vacuum and heated. The materials are then analyzed using XPS and XRD, after which the batteries were fabricated with Cr_2S_3 via a coin cell setup.

The results of electrode analysis indicate the formation of the SEI layer. Analysis of the electrodes proved a view into the underlying mechanism of SEI layer formation. Further testing including more cycling is necessary for further investigation.

In the immediate future XRD analysis like that shown above measured at the positions in the delithiation curve of samples 9, 10, and 11 need to be performed to reach a better understanding of the process.

REFERENCES

- (1) Cheung, T. T. X-Ray photoemission of Carbon: Lineshape Analysis and application to studies of Coals. *Journal of Applied Physics* **53**, 6857–6862 (1982).
<https://doi.org/10.1063/1.330025>
- (2) Choi, N. S., Chen,., Freunberger, S. A., Ji, X., Sun, Y. K., Amine, K., Yushin, G., Nazar, L. F., Cho, J., & Bruce, P. G. (2012). Challenges facing lithium batteries and electrical double-layer capacitors. In *Angewandte Chemie - International Edition* (Vol. 51, Issue 40, pp. 9994–10024). <https://doi.org/10.1002/anie.201201429>
- (3) Dedryvère, R. *et al.* XPS valence characterization of lithium salts as a tool to study electrode/electrolyte interfaces of Li-ion batteries. *The Journal of Physical Chemistry B* **110**, 12986–12992 (2006). <https://doi.org/10.1021/jp061624f>
- (4) Faber, Matthew S., et al. “Earth-Abundant Metal Pyrites (FES₂, COS₂, Nis₂, and Their Alloys) for Highly Efficient Hydrogen Evolution and Polysulfide Reduction Electrocatalysis.” *The Journal of Physical Chemistry C*, vol. 118, no. 37, 2014, pp. 21347–21356., <https://doi.org/10.1021/jp506288w>.
- (5) Ferretti, A. M., Mondini, S., & Ponti, A. (2016). Manganese Sulfide (MnS) Nanocrystals: Synthesis, Properties, and Applications. In *Advances in Colloid Science*. InTech. <https://doi.org/10.5772/65092>

- (6) Goodenough, J. B., & Park, K. S. (2013). The Li-ion rechargeable battery: A perspective. In *Journal of the American Chemical Society* (Vol. 135, Issue 4, pp. 1167–1176).
<https://doi.org/10.1021/ja3091438>
- (7) Hrbek, J., Xu, G.-Q., Sham, T. K. & Shek, M.-L. Interaction of potassium overlayers with oxygen and a potassium-dioxygen surface complex with carbon monoxide. *Vacuum* **41**, 153–156 (1990). [https://doi.org/10.1016/s0042-207x\(05\)80143-5](https://doi.org/10.1016/s0042-207x(05)80143-5)
- (8) Kim, Youngsik, and John B. Goodenough. “Lithium Insertion into Transition-Metal Monosulfides: Tuning the Position of the Metal 4s Band.” *The Journal of Physical Chemistry C*, vol. 112, no. 38, 2008, pp. 15060–15064.,
<https://doi.org/10.1021/jp8038847>.
- (9) Kim, Youngsik, et al. “Access to M^[SUP 3+]/m^[Sup 2+] Redox Couples in Layered Lims₂ Sulfides (M=Ti, v, CR) as Anodes for Li-Ion Battery.” *Journal of The Electrochemical Society*, vol. 156, no. 8, 2009, <https://doi.org/10.1149/1.3151856>.
- (10) Kim, Youngjin, et al. “SnSe Alloy as a Promising Anode Material for Na-Ion Batteries.” *Chemical Communications*, vol. 51, no. 1, 2015, pp. 50–53.,
<https://doi.org/10.1039/c4cc06106c>.
- (11) Li, M., Lu, J., Chen, Z., & Amine, K. (2018). 30 Years of Lithium-Ion Batteries. In *Advanced Materials* (Vol. 30, Issue 33). Wiley-VCH Verlag.
<https://doi.org/10.1002/adma.201800561>

- (12) Lu, J., Chen, Z., Pan, F., Cui, Y., & Amine, K. (2018). High-Performance Anode Materials for Rechargeable Lithium-Ion Batteries. *Electrochemical Energy Reviews*, 1(1), 35–53. <https://doi.org/10.1007/s41918-018-0001-4>
- (13) Moulder, J. F., Stickle, W. F., Sobol, P. E. and Bomben, K. D., 1992, *Handbook of X-Ray Photoelectron Spectroscopy*, Perkin-Elmer Corporation, Eden Prairie, MN, 261p.
- (14) Ogasawara, T., Debart, A., Holzapfel M., Novak, P., Bruce P. G., Am, J.. Chem. Soc. 2006, 128, 1390 – 1393; b) P. Poizot, S. Laruelle, S. Grugeon, L. Dupont, J. M. Tarascon, Nature 2000, 407, 496 – 499.
- (15) Park, S., Ahn, J., Kang, T., Park, S., Kim, Y., Cho, I., & Kim, J. (2020). Review of state-of-the-art battery state estimation technologies for battery management systems of stationary energy storage systems. *Journal of Power Electronics*, 20(6). <https://doi.org/10.1007/s43236-020-00122-7>
- (16) Prikhodchenko, Petr V., et al. “Nanocrystalline Tin Disulfide Coating of Reduced Graphene Oxide Produced by the Peroxostannate Deposition Route for Sodium Ion Battery Anodes.” *Journal of Materials Chemistry A*, vol. 2, no. 22, 2014, p. 8431., <https://doi.org/10.1039/c3ta15248k>.
- (17) Ren, W., Ma, W., Zhang, S., & Tang, B. (2019). Recent advances in shuttle effect inhibition for lithium sulfur batteries. In *Energy Storage Materials* (Vol. 23, pp. 707–732). Elsevier B.V. <https://doi.org/10.1016/j.ensm.2019.02.022>

- (18) Vaqueiro, P., Powell, A. v., Coldea, A. I., Steer, C. A., Marshall, I. M., Blundell, S. J., Singleton, J., & Ohtani, T. (2001). Colossal magnetoresistance in the layered chromium sulfide Cr_2S_3-x ($x=0.08$). *Physical Review B - Condensed Matter and Materials Physics*, 64(13), 1324021–1324024. <https://doi.org/10.1103/physrevb.64.132402>
- (19) V Watts, J. F. & Wolstenholme, J. *An introduction to surface analysis by XPS and AES*. (Wiley, 2020).
- (20) Xie, Junfeng, et al. “Defect-Rich MoS_2 Ultrathin Nanosheets with Additional Active Edge Sites for Enhanced Electrocatalytic Hydrogen Evolution.” *Advanced Materials*, vol. 25, no. 40, 2013, pp. 5807–5813., <https://doi.org/10.1002/adma.201302685>.
- (21) Xie, X., Wang, S., Kretschmer, K., & Wang, G. (2017). Two-dimensional layered compound based anode materials for lithium-ion batteries and sodium-ion batteries. *Journal of Colloid and Interface Science*, 499, 17–32. <https://doi.org/10.1016/j.jcis.2017.03.077>
- (22) Yang, F., Wang, D., Zhao, Y., Tsui, K. L., & Bae, S. J. (2018). A study of the relationship between coulombic efficiency and capacity degradation of commercial lithium-ion batteries. *Energy*, 145, 486–495. <https://doi.org/10.1016/j.energy.2017.12.144>
- (23) Zhang, Kai, et al. “Cobalt-Doped FeS_2 Nanospheres with Complete Solid Solubility as a High-Performance Anode Material for Sodium-Ion Batteries.” *Angewandte Chemie International Edition*, vol. 55, no. 41, 2016, pp. 12822–12826., <https://doi.org/10.1002/anie.201607469>.

- (24) Zhang, Y., Zhou, Q., Zhu, J., Yan, Q., Dou, S. X., & Sun, W. (2017). Nanostructured Metal Chalcogenides for Energy Storage and Electrocatalysis. In *Advanced Functional Materials* (Vol. 27, Issue 35). Wiley-VCH Verlag. <https://doi.org/10.1002/adfm.201702317>
- (25) Zhao, H., Deng, N., Yan, J., Kang, W., Ju, J., Ruan, Y., Wang, X., Zhuang, X., Li, Q., & Cheng, B. (2018). A review on anode for lithium-sulfur batteries: Progress and prospects. In *Chemical Engineering Journal* (Vol. 347, pp. 343–365). Elsevier B.V. <https://doi.org/10.1016/j.cej.2018.04.112>